Inorganic Chemistry

Article

pubs.acs.org/IC

In Situ XRD Study of $La_2Ni_7H_x$ During Hydrogen Absorption–Desorption

Kenji Iwase,*[,†] Kouji Sakaki,[‡] Yumiko Nakamura,[‡] and Etsuo Akiba[‡]

[†]Department of Materials Science and Engineering, Ibaraki University, 4-12-1, Nakanarusawa, Hitachi 316-8511, Japan

[‡]National Institute of Advanced Industrial Science and Technology (AIST), AIST Central-5, 1-1-1 Higashi, Tsukuba, Ibaraki 305-8565, Japan

ABSTRACT: Structural changes of $La_2Ni_7H_x$ during the first and second absorption–desorption processes along the *P*–*C* isotherm were investigated by in situ X-ray diffraction (XRD). Orthorhombic (*Pbcn*) and monoclinic (*C*2/*c*) hydrides coexisted in the first absorption plateau, but only a monoclinic (*C*2/*c*) hydride was observed in the first desorption plateau. Phase transformation of $La_2Ni_7H_x$ was irreversible between the first as well as the second absorption–desorption process. The lattice parameters and expansion of the La_2Ni_4 and $LaNi_5$ cells during the absorption–desorption process were refined using the Rietveld method. The lattice parameters *a* and *b* of the orthorhombic hydride (*Pbcn*) decreased, while the lattice parameter *c* increased with increasing hydrogen content in the first absorption. During the first absorption, the volume of the orthorhombic La_2Ni_4 cell expanded by more than 50%, while the expansion of the $LaNi_5$ cell was below 10%. The monoclinic La_2Ni_4 cell expanded to approximately four times the size of the $LaNi_5$ cell in the first absorption. The lattice parameters *a*, *b*, and *c* of the monoclinic hydride (*C*2/*c*) decreased with decreasing hydrogen content in the first desorption. These La_2Ni_4 and $LaNi_5$ cells contracted isotropically in the first desorption.

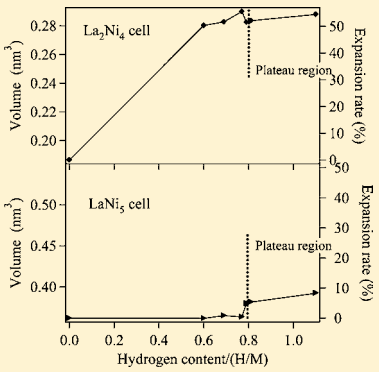

1. INTRODUCTION

Metal hydrides based on La–Ni intermetallic compounds have been extensively studied.[1−5] The La_2Ni_7 alloy has a hexagonal Ce_2Ni_7-type structure below 1268 K and a rhombohedral Gd_2Co_7-type structure between 1268 and 1287 K.[6] The unit cell of the Ce_2Ni_7-type structure contains two subunits, each of which consists of a $MgZn_2$-type cell and two $CaCu_5$-type cells stacking along the *c*-axis. The unit cell of the Gd_2Co_7-type structure is formed by stacking the three subunits. La_2Ni_7 and the related R_2Ni_7 hydride (R = rare earth) with a superlattice structure have been noticed as promising materials to serve as the negative electrode for nickel–metal hydride (Ni-MH) batteries.[7]

The crystal structure and hydrogen absorption properties of the Ce_2Ni_7 hydride have been reported by Denys et al.[8] The pressure–composition (*P*–*C*) isotherm of the hydride showed a flat plateau, in which the maximum hydrogen capacity reached 0.52 H/M at 293 K. The crystal structure of $Ce_2Ni_7D_{4.7}$ has been studied by in situ neutron diffraction, and it was found that $Ce_2Ni_7D_{4.7}$ belongs to the space group *Pmcn*. The unit cell expands along the *c*-axis, and the volume expansion of the Ce_2Ni_4 cell can be as high as 62–63%, while the volume of the $CeNi_5$ cell remains unchanged. All deuterium atoms are located in the Ce_2Ni_4 cell and on the boundary between the Ce_2Ni_4 and $CeNi_5$ cells.

Filinchuk et al. investigated the structural changes of Ce_2Ni_7 during hydrogenation by using synchrotron X-ray and neutron powder diffraction.[9] Ex situ diffraction data were used for Rietveld refinement. Using synchrotron XRD data, the space group of the metal sublattice of $Ce_2Ni_7H_x$ was determined to be *Pmcn*. The crystal structure of $Ce_2Ni_7D_{\sim 4}$ was refined using neutron powder diffraction data with the *Pmcn* and *Pmnm* models. The final refinement was obtained using *Pmcn* only. Deuterium atoms were located in the Ce_2Ni_4 cell or on the boundary between the Ce_2Ni_4 and $CeNi_5$ cells. The expansion of the Ce_2Ni_4 cell along the *c*-axis was approximately 60%, but the $CeNi_5$ cell was nearly unchanged.

The present authors previously reported the crystal structure of the metal sublattice of $La_2Ni_7H_x$ (x = 7.1, 10.8) determined by in situ XRD.[10] Two hydride phases were synthesized from a La_2Ni_7 alloy with a Ce_2Ni_7-type structure along the *P*–*C* isotherm. $La_2Ni_7H_{7.1}$ was orthorhombic (space group *Pbcn*), and the La_2Ni_4 and $LaNi_5$ cells expanded by approximately 50% and 5% from the alloy, respectively. $La_2Ni_7H_{10.8}$ was monoclinic (space group *C*2/*c*). The La_2Ni_4 and $LaNi_5$ cells expanded by 66% and 14%, respectively, from the alloy. The results indicate that a large expansion of the A_2B_4 cell along the *c*-axis is commonly observed in both Ce_2Ni_7 and La_2Ni_7, but the formation of a hydride phase with a higher hydrogen content, such as $La_2Ni_7H_{10.8}$, and expansion in AB_5 cells are observed only in La_2Ni_7.

Yartys et al. investigated the crystal structure of $La_2Ni_7D_{6.5}$ by ex situ neutron diffraction.[11] They reported that $La_2Ni_7D_{6.5}$ had the same hexagonal symmetry ($P6_3/mmc$) as the original alloy. The La_2Ni_4 cell expanded along the *c*-axis by 58.7%, and the

Received: June 4, 2013
Published: August 20, 2013

$LaNi_5$ cell slightly shrank by 0.5%. Deuterium atoms were located in the La_2Ni_4 cells and the boundary between the La_2Ni_4 and $LaNi_5$ cells, while the $LaNi_5$ cells were almost empty.

This Article presents recent results of in situ XRD measurements of $La_2Ni_7H_x$ during hydrogen absorption–desorption. The P–C isotherm of La_2Ni_7 was completed at 0.7 H/M, and the hydrogen atoms remained in the sample after the first desorption. To clarify the irreversible hydrogenation property between the first absorption and the first desorption, the lattice parameters and expansion of the La_2Ni_4 and $LaNi_5$ cells with increasing and decreasing hydrogen content were refined by the Rietveld method. The hydrogen occupation is related to the phase transformation during the hydrogen absorption–desorption process. The variation of the unit cell, the La_2Ni_4 and $LaNi_5$ cell volume, corresponds to the amount of hydrogen inserted into each of the cells. It is necessary to refine the structural parameters during hydrogen absorption–desorption process. This study presents the phase transformation and change of the structural parameters in the hydrogen absorption–desorption process.

2. EXPERIMENTAL SECTION

La_2Ni_7 alloy was prepared by arc-melting La and Ni metals (99.9%) in an Ar atmosphere. The annealing treatment was conducted at 1153 K for 120 h and quenched in ice water to obtain a single-phase alloy with a Ce_2Ni_7-type structure.

The sample for the P–C isotherm measurement was sealed in a stainless steel container, heated in a vacuum at 373 K for 1 h, and then kept at 273 K for 1 h. The P–C isotherm was measured using the Sieverts' method without pretreatment for activation. Before the second cycle measurement, the sample was evacuated at 273 K for 3 h.

The powder sample for XRD measurement was sieved to a particle size of <20 μm. The XRD data were collected using a Rigaku RINT 2500 V diffractometer. The operating condition was 50 kV × 200 mA with 0.5° divergence, scattering slits, and a 0.15-mm receiving slit.

In situ XRD was measured using a high-pressure chamber with Be windows and a temperature controller attached to the sample holder. The data were taken using Cu Kα radiation monochromatized with curved graphite in a step-scan mode of 2θ in the range 19°–95°. Approximately 1.8 g of the sample was placed in a stainless holder and covered with a 0.1-mm-thick Be plate to keep the sample surface flat during hydrogenation. The temperature was kept at 273 K during the measurement. To evaluate accurate lattice parameters, NIST Si (640 C) was used as an internal standard. The peak shift due to the volume change of the sample holder during the reaction was also calibrated using the internal standard. Data around $2\theta \sim 51°$, 71°, and 77° containing peaks of Be were excluded from refinement, while the diffraction of BeO, which often overlaps the sample's diffraction, was included in the refinement as the secondary phase. Structural parameters were refined using the Rietveld refinement program RIETAN-2000.[12−14] The reliability of the fitting was judged from the "goodness-of-fit" S; this was defined as $S = R_{wp}/R_e$, where R_{wp} is a residue of the weighted pattern and R_e is the statistically expected residue.

3. RESULTS

3.1. P–C Isotherm of La_2Ni_7. The P–C isotherm of La_2Ni_7 for the first absorption–desorption at 273 K is shown in Figure 1a. The first absorption was measured without any pretreatment for activation. The hysteresis factor [hereafter: Hf = $\ln(P_{abs}/P_{des})$] was 2.27, which was larger than that of $LaNi_5$ (Hf = 0.26).[15] The maximum hydrogen-storage capacity reached 1.24 H/M at hydrogen pressure 1.0 MPa. The P–C isotherm measurement for the desorption process was completed at 0.7 H/M and 0.003 MPa. The equilibrium pressures of the

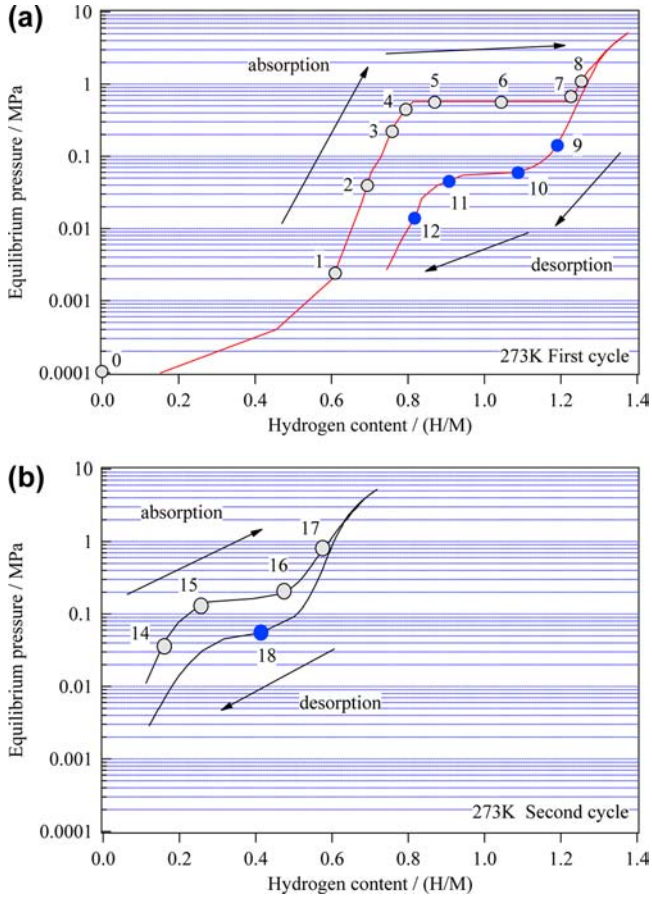

Figure 1. P–C isotherm of La_2Ni_7 at 273 K: (a) first cycle and (b) second cycle.

absorption and desorption plateaus were 0.57 and 0.06 MPa, respectively. Figure 1b shows the P–C isotherm of the second absorption–desorption at 273 K. The maximum hydrogen capacity reached approximately 1.4 H/M, including the hydrogen that remained in the material after the first desorption. The absorption and desorption plateaus were approximately 0.16 and 0.05 MPa, respectively. The equilibrium pressure and width of the second absorption plateau decreased in comparison to the first absorption. The Hf of the second cycle was 1.08, which is smaller than that of the first cycle, mainly because the absorption-plateau pressure significantly decreased.

3.2. In Situ XRD Profiles of First Absorption. In situ XRD profiles of $La_2Ni_7H_x$ ($0 \leq x \leq 10.8$) for the first absorption process are shown in Figure 2. The hydrogenation conditions for the XRD profiles from no. 0 to no. 8 correspond to the points indicated on the P–C isotherm in Figure 1a. The XRD profiles from no. 1 to no. 4 showed an orthorhombic phase and a peak shift with increasing hydrogen content. The XRD profiles of no. 5 and no. 6 in the plateau region showed coexisting orthorhombic and monoclinic phases, while those of no. 7 and no. 8 showed a monoclinic single phase. The observed orthorhombic phases and monoclinic phases are similar to those of $La_2Ni_7H_{7.1}$ and $La_2Ni_7H_{10.8}$ observed in our previous study.[10] The crystal structures of the metal sublattices of these two phases are shown in Figure 3.

3.3. In Situ XRD Profiles of First Desorption. The XRD profiles for the first desorption process are shown in Figure 4. No. 9 to no. 12 refer to the conditions indicated in Figure 1a.

dx.doi.org/10.1021/ic401419n | Inorg. Chem. 2013, 52, 10105−10111

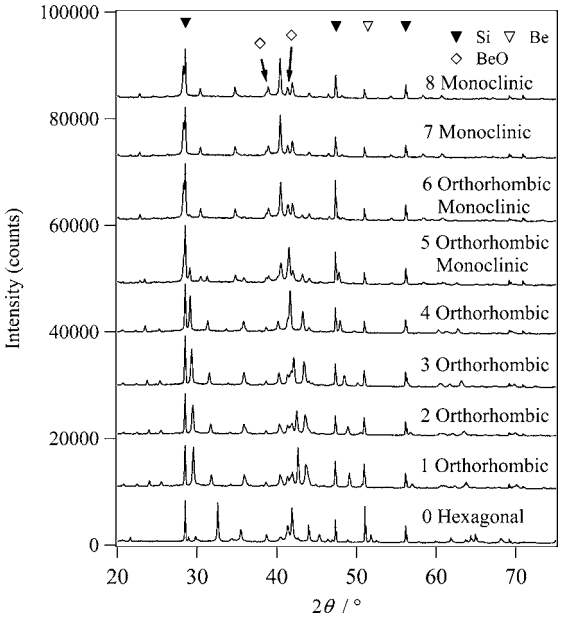

Figure 2. XRD profiles of $La_2Ni_7H_x$ ($0 < x < 10.8$) in the first absorption process.

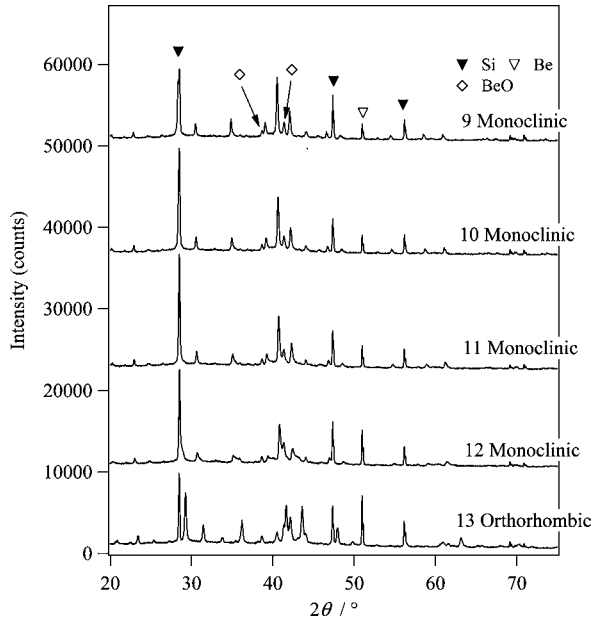

Figure 4. XRD profiles of $La_2Ni_7H_x$ ($0.8 < x < 10.8$) in the first desorption process.

Before collecting the XRD data of no. 13, the sample was evacuated at 273 K for 3 h. The XRD profiles for no. 9 to no. 12 are similar to those of the monoclinic phase seen in the absorption for no. 8. The peak position shifted to a higher angle, and the peak width increased with decreasing hydrogen content. $La_2Ni_7H_{7.3}$ (no. 12) had the largest peak width. In the plateau region for absorption, the orthorhombic and monoclinic phases coexisted in $La_2Ni_7H_{7.2-9.5}$ (no. 5 and no. 6). However, only the monoclinic phase was observed in $La_2Ni_7H_{10}$ (no. 10) and $La_2Ni_7H_{8.1}$ (no. 11) for the desorption plateau. Thus, the phase transformation of $La_2Ni_7H_x$ is irreversible during the first absorption−desorption process. Though the profile of no. 13 looked similar to an orthorhombic structure, the structure was not clear because of peak broadening. A hexagonal phase with a lower hydrogen content was not observed in the first desorption process.

3.4. Structure Parameters in First Absorption Process.

Figure 5 shows the refined pattern of $La_2Ni_7H_{7.2}$ (no. 5) with the two-phase model containing both the orthorhombic and monoclinic phases. The calculated pattern fit better with the observed pattern, and the goodness-of-fit S was 2.0.

Figure 6a,b shows the lattice parameters, cell volume of the orthorhombic phase for La_2Ni_4 and $LaNi_5$, and expansion of the axes and cells. The a and b axes shrank by approximately 1.0% while the c-axis expanded by more than 20%. During hydrogenation, the lattice expanded anisotropically from the alloy to the orthorhombic phase. The orthorhombic phase of the La_2Ni_4 cell expanded by over 50%, and the expansion in the $LaNi_5$ cell was less than 10%. It is interesting to note that the La_2Ni_4 cell volume decreased by over 0.7 H/M, in spite of the increasing hydrogen content. In contrast, the expansion of the $LaNi_5$ cell was below 0.9% and scarcely changed below 0.77 H/M, but it increased to 5.0% from 0.77 H/M to 0.79 H/M because of the sudden increase in b and c, as seen in Figure 6a.

Figure 7a,b shows the lattice parameters, volumes of the La_2Ni_4 and $LaNi_5$ cells in the monoclinic phase, and expansion of the axes and cells. The lattice parameters were almost

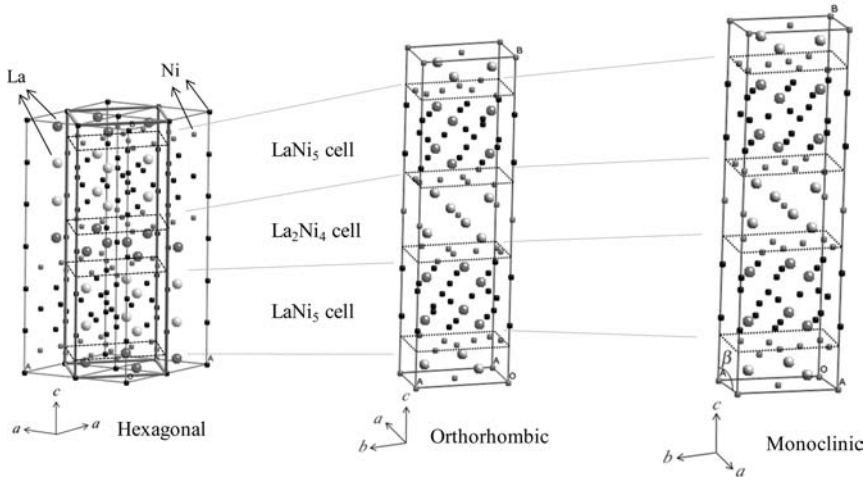

Figure 3. Crystal structures of metal sublattices of $La_2Ni_7H_x$ ($0 < x < 10.8$): hexagonal, orthorhombic, and monoclinic.

dx.doi.org/10.1021/ic401419n | Inorg. Chem. 2013, 52, 10105−10111

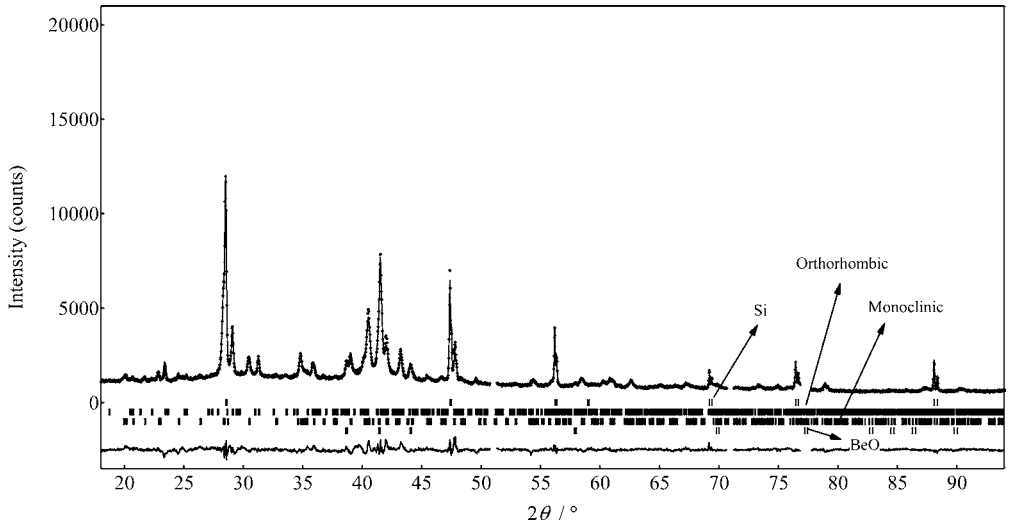

Figure 5. Rietveld refinement pattern of $La_2Ni_7H_{7.2}$ (no. 5) obtained in plateau region.

unchanged in the first absorption. The expansions of the La_2Ni_4 and $LaNi_5$ cells were 64% and 15%, respectively, as shown in Figure 7b. These values remained almost constant during the first absorption.

3.5. Structure Parameters in the Desorption Process. The structural parameters for the samples no. 9 to no. 12 were refined using a monoclinic structure model with the space group *C*2/*c*. The peak broadening for $La_2Ni_7H_{7.3}$ (no. 12) is wider than that for $La_2Ni_7H_{10.8}$ (no. 8), and β increases from 90.17(1)° in $La_2Ni_7H_{10.8}$ to 90.62(1)° in $La_2Ni_7H_{7.3}$. Monoclinic deformation of the metal sublattice increases with decreasing hydrogen content. The lattice parameters and their expansion rates in $La_2Ni_7H_x$ (no. 9 to no. 12) were plotted against hydrogen content, as shown in Figure 7a, where the rates were evaluated as expansion from the alloy phase before hydrogenation. The lattice parameters *a*, *b*, and *c* decreased with decreasing hydrogen content. The lattice parameter, *a*, of $La_2Ni_7H_{7.3}$ (no. 12) was smaller than that of the alloy by 0.8%.

The volumes of the La_2Ni_4 and $LaNi_5$ cells are plotted against hydrogen content in Figure 7b. As seen in the orthorhombic phase (Figure 6b), the La_2Ni_4 cell expanded to approximately four times the size of the $LaNi_5$ cell. The fact that the volume of the La_2Ni_4 and $LaNi_5$ cells decreases at low hydrogen content indicates that hydrogen occupation in both cells decreased with decreasing hydrogen content.

The orthorhombic structure model with the space group *Pbcn* was used for $La_2Ni_7H_{5.9}$ (no. 13). The refined lattice parameters *a*, *b*, and *c* were 0.4958(1), 0.8596(3), and 3.0350(1) nm; R_{wp} and R_I were 5.91% and 7.99%; and the *S* value was 2.7. The XRD of no. 13 had a broader profile than that of no. 1 to no. 4. The volume expansions of La_2Ni_4, $LaNi_5$, and the unit cell were 52.0%, 0.0%, and 17.9%, respectively, from the alloy.

3.6. In Situ XRD Profiles of Second Absorption–Desorption. XRD profiles for the second absorption–desorption process are shown in Figure 8. In the second absorption, $La_2Ni_7H_{7.3}$ (no. 14) and $La_2Ni_7H_{8.2}$ (no. 15) were in the orthorhombic phase, $La_2Ni_7H_{10}$ (no. 16) contained both the orthorhombic and monoclinic phases, and $La_2Ni_7H_{\sim 11}$ (no. 17) was a single monoclinic phase. In the second desorption, $La_2Ni_7H_{9.6}$ (no. 18) in the plateau region contained only a monoclinic phase, but $La_2Ni_7H_{\sim 6.8}$ (no. 19) was in an orthorhombic phase after evacuation at 273 K for 3 h. The phase transformations and structural changes were similar to those observed during the first absorption–desorption process.

The structure of $La_2Ni_7H_{\sim 11}$ (no. 17) was analyzed using a monoclinic model with the space group *C*2/*c*. The volume expansions of the La_2Ni_4, $LaNi_5$, and unit cells from the alloy were 63.5%, 14.3%, and 31.6%, respectively. These parameters were similar to those of $La_2Ni_7H_{10.8}$ (no. 8) from the first absorption.

The structure parameters of $La_2Ni_7H_{\sim 6.8}$ (no. 19) were refined using an orthorhombic model with the space group *Pbcn*. The volume expansion of the La_2Ni_4, $LaNi_5$, and unit cells, respectively, indicated 55.0%, 3.8%, and 21.0% expansion from the alloy. Peak broadening was observed in the XRD profile of $La_2Ni_7H_{\sim 6.8}$ (no. 19).

4. DISCUSSION

4.1. Phase Transformation in Absorption–Desorption. Chai et al. reported phase transformation of Ce_2Ni_7-type $La_{0.7}Mg_{0.3}Ni_{2.8}Co_{0.5}H_x$ by in situ XRD.[16] Rietveld refinement revealed that the metal sublattice of the full hydride phase had the same symmetry as that of the solid solution phase. The solid solution and hydride phases were observed in the absorption plateau, while only the hydride phase was observed in the desorption plateau. Although $La_{0.7}Mg_{0.3}Ni_{2.8}Co_{0.5}$ and La_2Ni_7 are different in their phase transformation and structural changes during absorption, both compounds had a similar desorption behavior, i.e., without a two-phase state.

In this study, the phase transformation of La_2Ni_7 followed the order hexagonal → orthorhombic → monoclinic for the first absorption, and the two-phase region (orthorhombic + monoclinic) was observed in the *P*–*C* isotherm plateau. The crystal structure of the hydride phase remained monoclinic during the first desorption. Only the monoclinic phase was observed in the plateau region, in which the lattice parameter continuously decreased with the hydrogen content. Similar phase transformations were observed in the second absorption and desorption. The phase transformation of $La_2Ni_7H_x$ was not reversible between absorption and desorption, as shown in Table 1.

dx.doi.org/10.1021/ic401419n | *Inorg. Chem.* 2013, 52, 10105–10111

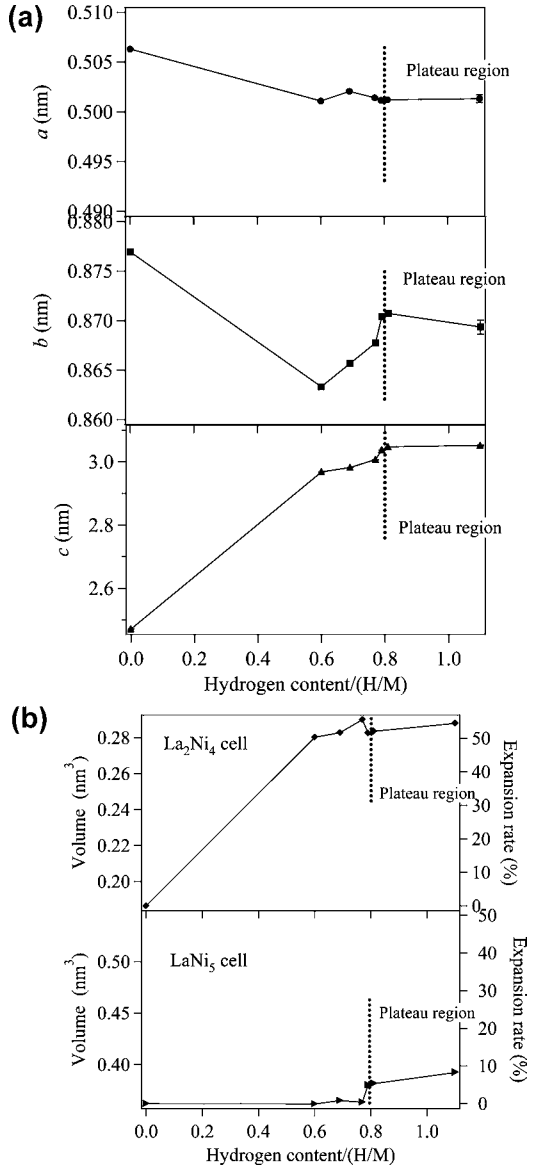

Figure 6. Dependence of lattice parameters, unit cell volume, La_2Ni_4 and $LaNi_5$ cell volumes, and their expansion rates from the alloy on hydrogen content in orthorhombic phase at the first absorption–desorption process: (a) lattice parameters *a*, *b*, *c*; (b) La_2Ni_4 and $LaNi_5$ cell volume.

In the first absorption, the metal sublattice of orthorhombic shrank 0.7–1.6% along the *a* and *b* axes, but the *c* axis expanded over 20% from the alloy. The lattice parameters *a* and *b* indicated the increase and decrease with increasing hydrogen content. The expansion of *c* axis was relaxed by the shrink of *a* and *b* axes. The expansion rate of $LaNi_5$ cell volume was under 10%, which is smaller than that of the La_2Ni_4 cell (~50%). The phase transformation from the alloy to orthorhombic is complex. The orthorhombic is stable with the anisotropic expansion of the metal sublattice. The orthorhombic transformed to monoclinic over 0.71 H/M. The metal sublattice of monoclinic expanded isotropically from orthothombic, but the expansion of La_2Ni_4 cell volume (14.0%) is larger than that of $LaNi_5$ cell (5.8%).[10] The phase transformation form orthorhombic to monoclinic is simple.

Only the monoclinic phase was observed in the first desorption. The volume expansion of the La_2Ni_4 and $LaNi_5$ cells in no. 12 was 59.2% and 8.9%, as shown in Figure 7b. Hydrogen atoms were distributed in both the La_2Ni_4 and $LaNi_5$ cells, and stable hydrogen occupation sites exist in both the cells. The volume of the La_2Ni_4 and $LaNi_5$ cells isotropically contracts, and the hydrogen atoms are gradually released from the La_2Ni_4 and $LaNi_5$ cells. The lattice parameters and the volume of the La_2Ni_4 and $LaNi_5$ cells in the monoclinic phase isotropically decreased during the first desorption. In contrast, the lattice parameters expanded isotropically during the phase transformation from orthorhombic to monoclinic in the first absorption, but the volume of the La_2Ni_4 and $LaNi_5$ cells increased anisotropically.[10] This comparison suggests that the hydrogen occupation in the monoclinic La_2Ni_4 and $LaNi_5$ cells during the desorption process is more stable than in the orthorhombic. The *P*–*C* isotherm shows that the hydrogen atoms remain in the La_2Ni_4 and $LaNi_5$ cells, in which the hydrogen-occupation sites are significantly more stable.

The phase transformation of metal sublattice of $La_2Ni_7H_x$ is irreversible during absorption–desorption process. Hydrogen occupation in the La_2Ni_4 and $LaNi_5$ cells affects the phase transformation between orthorhombic and monoclinic. We focused on the hydrogen occupation of the La_3Ni_3 and La_3Ni_1 sites in the La_2Ni_4 cell. The volumes of the La_3Ni_3 and La_3Ni_1 sites in the La_2Ni_4 cell expanded approximaterly 40% and 150% during the phase transformation from hexagonal to monoclinic. The monoclinic phase does not transform to orthorhombic in the desorption process. Hydrogen occupation in both the La_2Ni_4 and $LaNi_5$ cells affects the phase transformation. To determine the hydrogen occupation in the La_2Ni_4 and $LaNi_5$ cells, an in situ neutron powder diffraction study is under way.

4.2. Expansion of La_2Ni_4, $LaNi_5$, and Unit Cells. The lattice parameters and unit cell expanded anisotropically with increasing hydrogen content. Considering the volume expansion of the La_2Ni_4 and $LaNi_5$ cells shown in Figure 6 b, most of the hydrogen occupies the La_2Ni_4 cell, and only a small fraction of hydrogen is located in the $LaNi_5$ cell.

The lattice parameters *a*, *b*, and *c*, and unit cell volume of the monoclinic phase, were almost constant in the first absorption. The cell volume of La_2Ni_4 increased while that of $LaNi_5$ decreased for hydrogen content greater than 1.1 H/M. The unit cell volume relaxed with the shrinking of the $LaNi_5$ cell (Figure 7b). This is likely caused by an increase in the hydrogen occupation of the La_2Ni_4 cell and the accompanying decrease in the $LaNi_5$ cell. It may be related to a rearrangement of the hydrogen occupation near the boundary between the La_2Ni_4 and $LaNi_5$ cells. In the first desorption, the lattice parameters *a*, *b*, and *c* decrease isotropically with decreasing hydrogen content. The same tendency was also seen in the volume of the La_2Ni_4 and $LaNi_5$ cells.

The *P*–*C* isotherm indicated that approximately 0.7 H/M of hydrogen remained in the sample at the end of the first desorption. Considering the expansion of the La_2Ni_4 and $LaNi_5$ cells of $La_2Ni_7H_{7.2}$ (no. 12), obtained after desorption, the hydrogen content of the La_2Ni_4 cell was larger than that of the $LaNi_5$ cell. Assuming that the $LaNi_5$ cell expanded in proportion to the hydrogen content for both $LaNi_5H_{\sim 7}$ and $La_2Ni_7H_{7.2}$ (no. 12), the residual hydrogen content in the $LaNi_5$ cell in $La_2Ni_7H_{7.2}$ would be approximately 0.25 H/M ($LaNi_5H_{\sim 1.5}$); approximately 30% and 70% of the total amount of the residual hydrogen in $La_2Ni_7H_{7.2}$ are located in the $LaNi_5$ and La_2Ni_4 cells, respectively.

4.3. Lattice Strain Introduced by Hydrogen Absorption and Desorption. Significant peak broadening, caused by

dx.doi.org/10.1021/ic401419n | *Inorg. Chem.* 2013, 52, 10105–10111

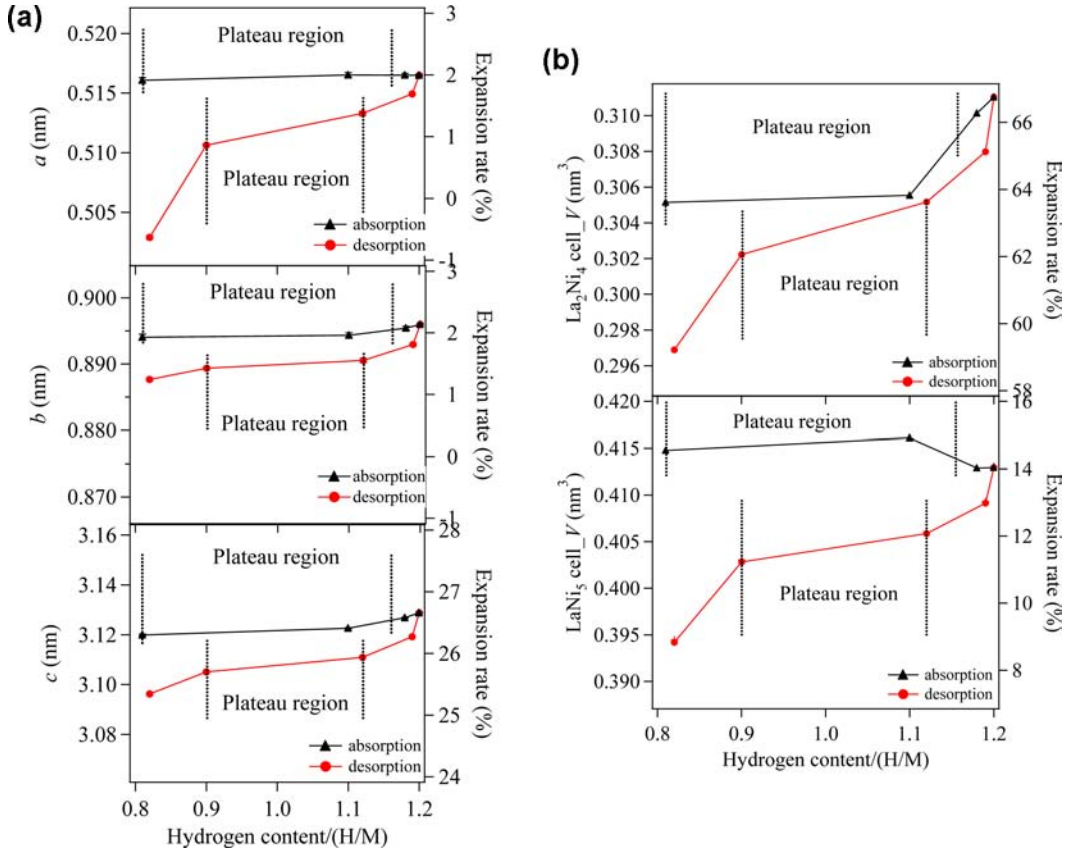

Figure 7. Dependence of lattice parameters, unit cell volume, La_2Ni_4 and $LaNi_5$ cell volumes, and their expansion rates from the alloy on hydrogen content in monoclinic phase at the first absorption−desorption process: (a) lattice parameters *a*, *b*, *c*; (b) La_2Ni_4 and $LaNi_5$ cell volume.

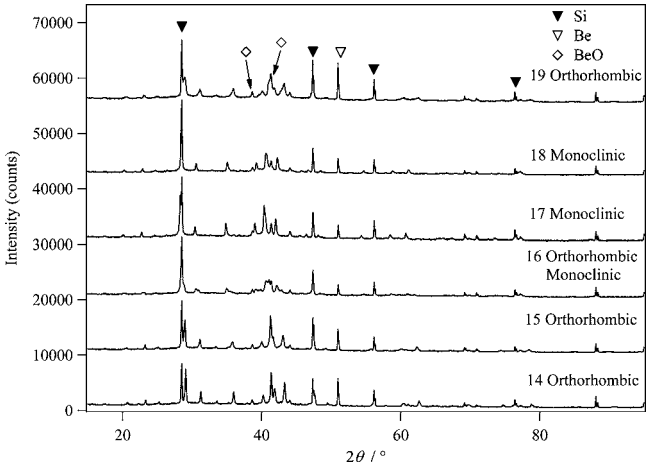

Figure 8. XRD profiles of $La_2Ni_7H_x$ in the second absorption−desorption process.

dense lattice defects, is observed in the diffraction pattern of $LaNi_5$ after hydrogenation.[17] The peak broadening observed for the first absorption of La_2Ni_7 was not as significant as that for $LaNi_5$. It is implied that stacking of La_2Ni_4 cells prevents lattice defects and strain. The peak broadening observed in the second desorption is larger than that in the first desorption. This indicates that repeating absorption and desorption can gradually induce lattice strain.

Some of the authors reported that the anisotropic lattice strain of the hydride phase of $LaNi_5$ is approximately 2.0−2.5%, with the anisotropic broadening vector of ⟨110⟩, in the first

Table 1. Structural Model for Rietveld Refinement at Various Hydrogen Content in the First and Second Absorption−Desorption[a]

point	process	hydrogen content	space group
no. 1−no. 4	first absorption	$5.4 \le x \le 7.1$	*Pbcn*
no. 5−no. 6	first absorption	$7.3 \le x \le 9.5$	*Pbcn*, *C*2/*c* (two phase)
no. 7−no. 8	first absorption	$10.7 \le x \le 10.8$	*C*2/*c*
no. 9−no. 12	first desorption	$7.2 \le x \le 10.6$	*C*2/*c*
no. 13	first desorption (after evacuation)	$x = 5.9$	*Pbcn*
no. 14−no. 15	second absorption	$1.5 \le x \le 2.3$	*Pbcn*
no. 16	second absorption	$x = 4.2$	*Pbcn*, *C*2/*c* (two phase)
no. 17	second absorption	$x = 5.2$	*C*2/*c*
no. 18	second desorption	$x = 3.7$	*C*2/*c*
no. 19	second desorption	$x < 3.7$	*Pbcn*

[a]Point corresponds to numbers indicated in Figure 1a,b.

absorption by in situ XRD.[18] The Rietveld refinement was used as a pseudo-Voigt function, containing a Gaussian function and a Lorentzian function.[19,20] Anisotropic strain was calculated using the Lorentzian parameter. In the $La_2Ni_7H_x$ of this study, the anisotropic strain obtained using the same method was much smaller, 0.1−0.4% in the orthorhombic phase and 0.1−0.7% in the monoclinic phase for the first absorption with an anisotropic broadening vector of ⟨001⟩. Isotropic strain was

dx.doi.org/10.1021/ic401419n | *Inorg. Chem.* 2013, 52, 10105−10111

approximately 0.5%, which is also smaller than the 2.0% observed in $LaNi_5$.

5. CONCLUSIONS

In the first absorption process, the crystal structure transformation follows the order hexagonal → orthorhombic → monoclinic with increasing hydrogen content; however, only the monoclinic form was observed in the first desorption. The phase transformation for $La_2Ni_7H_x$ was not reversible between the first absorption and desorption process with accompanying by anisotropic lattice expansion.

The monoclinic phase has stable hydrogen-occupation sites in both the La_2Ni_4 and $LaNi_5$ cells and does not release hydrogen under ambient conditions. The monoclinic phase does not transform to orthorhombic during the first desorption. The same phenomenon was also observed in the second absorption−desorption process.

AUTHOR INFORMATION

Corresponding Author

*E-mail: fbiwase@mx.ibaraki.ac.jp. Phone: +81-29-352-3233. Fax: +81-29-287-7189.

Notes

The authors declare no competing financial interest.

ACKNOWLEDGMENTS

The authors thank Emeritus Professor H. Asano (University of Tsukuba) and Dr. H. Enoki (AIST) for their helpful advice. A part of this work was supported by the New Energy and Industrial Technology Development Organization (NEDO) under "Advanced Fundamental Research on Hydrogen Storage Materials (Hydro-Star)".

REFERENCES

(1) Oesterreicher, H.; Clinton, J.; Bittner, H. *Mater. Res. Bull.* **1976**, *11*, 1241−1248.
(2) Buschow, K. H. J.; Vanmal, H. H. *J. Less-Common Met.* **1972**, *29*, 203−210.
(3) Yamamoto, T.; Inui, H.; Yamaguchi, M.; Sato, K.; Fujitani, S.; Yonezu, I.; Nishio, K. *Acta Mater.* **1997**, 5213−5221.
(4) Buschow, K. H. J.; Van Der Goot, A. S. *J. Less-Common Met.* **1970**, *22*, 419−428.
(5) Virkar, A. V.; Raman, A. *J. Less-Common Met.* **1969**, *18*, 59−66.
(6) *Binary Alloy Phase Diagrams*, 2nd edition plus updates; Okamoto, H., Ed.; ASM International: Materials Park, OH, 1996.
(7) Yasuoka, S.; Magari, Y.; Murata, T.; Tanaka, T.; Ishida, J.; Nakamura, H.; Nohma, T.; Kihara, M.; Baba, Y.; Teraoka, H. *J. Power Sources.* **2006**, *156*, 662−666.
(8) Denys, R. V.; Yartys, V. A.; Sato, M.; Riabov, A. B.; Delaplane, R. G. *J. Solid State Chem.* **2007**, *180*, 2566−2576.
(9) Filinchuk, Y. E.; Yvon, K.; Emerich, H. *Inorg. Chem.* **2007**, *46*, 2914−2920.
(10) Iwase, K.; Sakaki, K.; Nakamura, Y.; Akiba, E. *Inorg. Chem.* **2010**, *49*, 8763−8768.
(11) Yartys, V. A.; Riabov, A. B.; Denys, R. V.; Sato, M.; Delaplane, R. G. *J. Alloys Compd.* **2006**, *408−412*, 273−279.
(12) Izumi, F. http://homepage.mac.com/fujioizumi/.
(13) Izumi, F. *Rigaku J.* **2000**, *17*, 34−45.
(14) Izumi, F.; Young, R. A. *The Rietveld Method*; International Union of Crystallography; Oxford University Press: Oxford, U.K., 1993; p 13.
(15) Osumi, Y.; Suzuki, H.; Kato, A.; Oguro, K.; Kawai, S.; Kaneko, M. *J. Less-Common Met.* **1983**, *89*, 287−292.
(16) Chai, Y.; Asano, K.; Sakaki, S.; Enoki, H.; Akiba, E. *J. Alloys Compd.* **2009**, *485*, 174−180.
(17) Nakamura, Y.; Oguro, K.; Uehara, I.; Akiba, E. *Int. J. Hydrogen Energy* **2000**, *25*, 531−537.
(18) Nakamura, Y.; Akiba, E. *J. Alloys Compd.* **2000**, *308*, 309−318.
(19) Larson, A. C.; Dreele, R. B. *Von. GSAS-General Structure Analysis System*; Report LAUR 86-748; Los Alamos National Laboratory: Los Alamos, NM, 1994; pp 127−138.
(20) Bish, D. L. *Modern Powder Diffraction*; Reviews of Mineralogy, Vol. *20*; Mineralogical Society of America: Washington, DC, 1989.